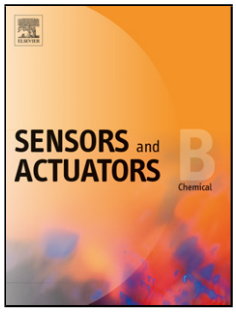

Title: Printed Flexible Electrochemical pH Sensors based on CuO Nanorods

Authors: Libu Manjakkal, Bhuvaneshwari Sakthivel, Nammalvar Gopalakrishnan, Ravinder Dahiya

PII: S0925-4005(18)30370-8
DOI: https://doi.org/10.1016/j.snb.2018.02.092
Reference: SNB 24187

To appear in: *Sensors and Actuators B*

Received date: 6-10-2017
Revised date: 21-1-2018
Accepted date: 10-2-2018

Please cite this article as: Libu Manjakkal, Bhuvaneshwari Sakthivel, Nammalvar Gopalakrishnan, Ravinder Dahiya, Printed Flexible Electrochemical pH Sensors based on CuO Nanorods, Sensors and Actuators B: Chemical https://doi.org/10.1016/j.snb.2018.02.092

Printed Flexible Electrochemical pH Sensors based on CuO Nanorods

Libu Manjakkal[a], Bhuvaneshwari Sakthivel[b], Nammalvar Gopalakrishnan[b], Ravinder Dahiya[a*]

[a]Bendable Electronics and Sensing Technologies (BEST) Group, School of Engineering, University of Glasgow, G12 8QQ, U.K.

[b]Thin Film Laboratory, National Institute of Technology, Tiruchirappalli-620015, India

*Corresponding author : Email: Ravinder.Dahiya@glasgow.ac.uk

Graphical abstract

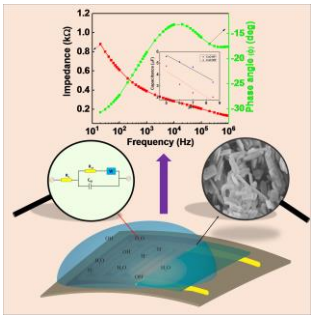

Highlights

- CuO nanorods and CuO nanoflower were prepared by hydrothermal synthesis method.
- New flexible capacitive pH sensors were fabricated by using CuO nanostructures.
- Microstructure, morphology and crystal structure of the nanomaterial were investigated.
- The pH sensing performance was proved by electrochemical impedance spectroscopic analysis.
- The sensor performance under different flexible conditions were tested
- The sensor performance in biomedical application were tested.

Abstract

Nanostructured metal oxides have attracted significant interest in a range of areas in electrochemical applications such as sensors, supercapacitors, and battery electrodes etc. Printing of these materials on flexible substrates will open new applications for the fabrication of sensors for monitoring the biological-food-medicine-agricultural systems. This paper presents the printed CuO based flexible electrochemical pH sensors. The sensors with interdigitated electrodes, screen printed on flexible substrates, are based on CuO nanostructures having nanorods (NR) morphology. The morphology influences the charge transfer phenomena and hence the sensor performance, as confirmed by the electrochemical studies. The NR based sensors have better stability with respect to conventional nanoflowers (NF). The structural analysis shows NRs exhibit high crystallinity and low surface roughness (130 nm) with respect to NF (192 nm). The sensor capacitance in the test frequency range (20 Hz -10 MHz) decreases exponentially with increase in pH. The CuO NR based sensor exhibits a sensitivity of 0.64µF/pH in the range pH 5-8.5. The sensor performance towards interfrence to other ions and analytes such as Na^+, K^+, glucose, and urea was found to have negligible influence (±1.5 nF) on the sensing electrode. The capacitance of sensors is also found to vary with different bending conditions.

Keywords: CuO; Nanostructures; Flexible; Capacitive; pH sensor; Biomedical applications

1. Introduction

Miniaturized electrochemical pH sensors received significant attractions in many fields including water quality monitoring [1] and biomedical applications [2, 3] due to its high sensitivity, fast response and economic with the lower cost of fabrication. The value of pH reflects the state of many physiological, biological and medical conditions. Recently, the need for electrochemical pH sensors in wearable systems has been felt for applications such as wound monitoring and sweat or tears based health analysis etc. [2, 3]. The sensors in these emerging applications should be flexible (i.e. physically bendable), in addition to being sensitive, fast, and biocompatible. In this regard, a range of materials and designs have been explored, but the semiconducting metal oxides (SMOs) are particularly attractive as they allow fabricating miniaturized sensors with very fast response and excellent sensitivity on the variety of substrates and production can be scaled up [4-6]. Owing to high electrochemical performances, the pH sensors from these materials have better stability and can be fabricated

in different design based on method of operation [6]. Further, in the form of nanostructures, the SMOs are known to have better optical, chemical and mechanical properties than their bulk counterparts. The nanostructured CuO is particularly attractive as it offers electron transfer at the lower potential, is non-toxic and it is relatively easy to synthesis them with various morphologies and dimension [7-10]. As a p-type semiconductor (indirect bandgap of 1.2 eV and a direct band gap of 3.2–3.3 eV [10] the CuO is chemically stable, inexpensive, and abundant and for this reason it attracted attention in numerous applications such as gas sensors [11, 12], supercapacitor electrodes [7], and antimicrobial materials [13].

Here we present the flexible or bendable pH sensors based on CuO nanostructures, particularly with nanorods (NRs) morphology. The dimension and morphology of NRs were controlled by tuning the solvent, reaction temperature and the duration of synthesis [10]. The morphology of nanostructures has been found to have a profound impact on sensor's performance [8, 9, 14]. As an example, CuO nanoflower (NF) based pH sensors have been shown to have a sub-Nernstian response of 28 mV/pH in a wide pH range of 2-11 [9]. The high surface to volume ratio of nanostructure such as nanoribbons, nanotubes, and nanoleaves etc. offers large reactive sites and for this reason the sensors from them could have enhanced sensitivity, and selectivity [10, 14-16]. For this sake of comparison, the CuO nanostructures with NF morphology have also been explored in this paper. It is noted that the NR based sensors show high sensitivity than those based on NF, especially in the pH range (i.e. 5-11) relevant for biological-food-medicine-agricultural applications. The pH sensors have been designed to have interdigitated electrode (IDE) structure and realized with low-cost screen printing method [17, 18]. The fabrication by printing overcomes the thermal budget issues as it is carried out at low temperatures compatible with flexible substrates such as plastic, polymers etc. Further, IDE structure-based sensors do not require reference electrode [4, 18]. A detailed investigation of the structural and morphological properties of the CuO NR and NF materials were carried out. The electrochemical properties have been evaluated for the first time for this type of pH sensors using electrochemical impedance spectroscopic (EIS) analysis. To demonstrate the efficacy of presented sensors for different application, we have also evaluated the CuO NR based sensor in a pH range of 5-9 (which is important for water and food quality etc.). To analysis the performance of sensor in different type of solution we tested the sensitivity in concentrated Dulbecco's Modified Eagle Medium (DMEM) and standard buffer solutions. Further, the influence of bending on the performance of flexible sensors have been evaluated.

2. Materials and Methods

2.1.Synthesis of CuO nanostructures and fabrication of sensors

The CuO NF and NR powders were prepared by low temperature hydrothermal synthesis method. The size and morphology of nanostructures were varied by changing the solvent, reaction temperature and the duration of synthesis. The CuO NFs were obtained from 0.1 M Copper(II) nitrate hemi(pentahydrate) ($Cu(NO_3)_2 \cdot 2.5H_2O$, Alfa Aesar, 98 % purity) and 0.7 M of NaOH (Alfa aesar, 98 % purity) mixed in 35 ml de-ionized water and 40 ml ethylene glycol under vigorous stirring for 60 min. The dark blue solution obtained from this step was transferred to a Teflon lined autoclave and kept in the furnace for 10 h at 140°C. Following this the precipitate was washed by centrifugation with water and ethanol several times and dried in air for 24 h. For CuO NRs, a 75 ml of deionized water solvent was used, and the Teflon lined autoclave was kept in furnace for 12 h at 160°C. The washing and drying was same as for CuO NF. The methods for synthesis of CuO NF and NR are shown in Fig. 1a.

For the fabrication of the pH sensors, first, the IDE structure (with finger length 10 mm, electrode width 0.5 mm and spacing between fingers 0.5 mm) was realized on both alumina and flexible Polyethylene terephthalate (PET) substrate by using screen printing method. The Ag paste (DuPont 5000)), which can be fired at low temperature, was used for this purpose. After printing, the IDE layers were dried at 120°C for 20 min. For sensitive layer, the pastes of CuO NF and NR were prepared by mixing of corresponding CuO nanopowders with 40 wt.% copolymer of poly (methyl methacrylate) (PMMA) – poly (butyl methacrylate) (PMBA) function as binder and butyl carbitol acetate (BCA) as solvent in an agate mortar for 1 h. The CuO NR and CuO NF paste was then screen printed on the top of IDE electrodes over an area of 18×13 mm^2 and dried at 120°C for 2 h. The schematic representation of pH sensor and the image of a flexible sensor are shown in Fig. 1b and 1c.

2.2.Characterization methods

Field emission scanning electron microscopy (FESEM, Zeiss ULTRA 55) was employed for the morphological and constituent elemental analysis. The quantitative measures such as grain size and structure of NR and NF were measured by using Transmission Electron Microscopy (TEM, Philips CM 200). The selected area (electron) diffraction (SAED) pattern of TEM image indicates the crystalline structure. The crystal structure and phase analysis of the CuO NF and CuO NR were carried out using X-ray diffractometer (XRD, Rigaku Ultima III, with Cu K_α (λ=1.514 Å). The structural properties of NR and NF were confirmed using micro Raman spectrometer (Renishaw, RM 2000,) with the 514.5 nm line of an argon ion laser

as the exciting light source with 5 mW power. A Perkin-Elmer 'Spectrum RX-FT-IR' spectrometer (USA) was utilized for vibration spectroscopy and functional group analysis of the materials. QuantachromeNova-1000 surface analyser at liquid nitrogen temperature was employed for the determination of surface area and porosity of the material. N_2 adsorption–desorption isotherm cycle measurements for CuO NF and NR were performed up to the saturation vapour pressure of nitrogen at −196 °C. The pore size distribution of the materials was determined from the adsorption data using BJH and de Boer's t-method. The surface morphology and roughness of the CuO films with scan size 10 μm with the scan rate of 0.5 Hz were investigated by using atomic force microscopy (AFM) (Park System's NX-10, South Korea) using a silicon nitride cantilever in non-contact mode.

The electrochemical sensing performance of the fabricated CuO NF and NR electrode was evaluated by using test solutions with pH ranging from 3 to 11 and buffer solutions (pH range 5-9). The solutions were prepared by adding 1 mol% of HCl or KOH into distilled water. The simple two-electrode configuration of the electrochemical cell allow evaluation of the sensing performance of CuO NF and CuO NR sensors by EIS analysis. A standard glass electrode pH meter (HI 98130, HANNA) with temperature and conductivity probe was applied to control the pH levels, temperature and the conductivity value of each pH test solutions. Prior to the measuring the electrochemical properties of CuO NF and NR films at different pH values of test solutions, the sensors were dipped in a solution for 10 min for stabilization. After each measurement, the sensitive layer was washed with deionized water and dried with a paper towel to reduce the contamination of sensitive electrode surface by the solution of another pH. The electrochemical performance of the sensors by EIS analysis was carried out by using KEYSIGHT LCR meter in the frequency range 20 Hz-10 MHz. The performance of sensors in different bending conditions was investigated by placing the sensors on the cylindrical surfaces of the radius of curvatures 5 and 10 mm. Finally, the performance of sensors was evaluated for application in the range of pH 5 to 9 by using a sample with concentrated DMEM (Sigma-Aldrich). The effect of interference of other analytes (e.g. glucose, urea) and ions (e.g. Na^+ and K^+) on the capacitance of the flexible pH sensor was studied and comapred in test solutions containing 0.01 M of these analytes and cations. For this purpose, the potential of applied sinusoidal signal was varied between 5, 10, 50 and 100mV and the corresponding variation in the impedance was studied.

3. Results and Discussion

3.1.Structural and morphological analysis of CuO NF and NR

The morphology of CuO NF and CuO NR with FESEM and TEM images is shown in Fig. 2. The NF and NR morphologies of CuO nanostructures can be clearly seen in the Fig. 2a and 2d respectively. Fig. 2a confirms the formation of NF in large scale with stacked nanosheets as primary units. The FESEM image in Fig. 2d show nearly uniform, blunt edged and transparent NR–shaped CuO nanostructure. Fig. 2b and 2c shows the TEM and SAED patterns of the CuO NF sample. The TEM image further confirms the formation of NFs with an average diameter of 1 μm and consist of uniform nanosheets with a thickness of 21 nm. The rings are shown in the Fig. 2c SAED pattern indicate the polycrystalline nature of the sample. The indexed planes are in accordance with the reported planes and the XRD analysis in Fig. 3a. Likewise, the TEM images in Fig. 2e show the well-defined blunt edged NRs that are quite transparent and form a stacking pattern. The NRs are about 450 nm wide and have a length of 950 nm and thickness of 45 nm. The SAED pattern in Fig. 2f shows the single crystallinity of the NRs and indexed according to the JCPDS card no. 45-0937. Thus, the morphological analysis reveals well crystallinity of CuO nanostructures.

The crystalline phase of the as-prepared nano-powder of CuO NF and NR are revealed in XRD spectra of Fig. 3a and 3b. The observed peaks of CuO nano-powders and films indicate the monoclinic structure (JCPDS 45-0937). The absence of peaks due to impurities indicate that the crystal structures of CuO are phase pure and well crystalline. The broader peaks indicate the nano-crystalline nature of CuO NF and CuO NR. The sharp intense peaks observed in the case of CuO NR as compared to CuO NF could be due to the crystalline cluster of NR. The XRD spectra observed for the films of CuO NR and NF exhibited similar peaks that belong to the monoclinic structure of CuO. The micro Raman spectra recorded for CuO NF and NR films are shown in Fig. 3c and 3d. The monoclinic phase of CuO belongs to the space group of C^6_{2h}, where the primitive cell contains two molecular units. Thus, it can be said from the selection rule that there are twelve vibrational modes at zone centre, including three acoustic modes (A_u+2B_u), six IR active modes (3A_u+3B_u) and three Raman active modes (A_g+2B_g) [19]. Based on the group theory, these lattice vibrations at the Γ point of the Brillioun zone are given by:

$$\Gamma = 4Au + 5Bu + Ag + 2Bg \qquad (1)$$

From Fig. 3c, it is seen that the peaks are broadened and downshifted compared to the CuO single crystal vibrations. The spectrum shows three peaks at 268, 321 and 564 cm^{-1}. The A_g mode observed at 268 cm^{-1} is associated with the in-phase/out-phase rotation of the CuO

asymmetric stretching mode while B_{1g} bending mode existing at 321 cm^{-1}. The B_{2g} mode observed at 564 cm^{-1} is associated with the symmetric oxygen stretching. The three active Raman modes identified here are comparable with the literature [20-22]. In the case of NR film (Fig. 3d) the three vibrational modes found to shift towards the higher wavenumber and observed at 271, 330 and 616 cm^{-1}. These significant peaks also indicate the single phase and good crystallinity of the as-synthesized CuO nanostructures. The shift in peak position may be attributed to the difference in morphology caused by the reaction temperature and duration. In addition to that, the state of agglomeration is also found to influence the Raman properties of nanoparticles. The increase of agglomeration can result in a red-shift and broadening of the peaks, which is also observed with increase in the temperature and the reduction in particle size. The red shifting of NF in Fig.3c, as compared to NR (Fig. 3d), can be explained by the flower-like morphology, which is a collection of sheet-like structures. Further, the sub-micron size of the rectangle-like structures can also contribute to the shift in peak and result in the broadening of peaks through quantum confinement effect of CuO nanostructures (esp. with <1 μm flower-like structures). It may be noted that irrespective of the binders used during screen printing, the presence of three vibrational modes corresponding to CuO rules out the existence of impurities or binder left over.

The FT-IR spectrum for the CuO nanostructures in Fig. 3e shows three signature peaks at 418, 496 and 603 cm^{-1} which belong to the A_u, B_u and the other B_u mode of CuO in the case of NR. However, for NF a sharp peak at 514 was observed along with weak peaks on either side. The high-frequency peak at 603 cm^{-1} may be attributed to the Cu-O stretching along (101) direction. The absence of peaks in the range 605-660 cm^{-1} rule out the existence of Cu_2O phase and confirms the formation of CuO phase [21].

The pore size of nanostructures also strongly influences the electrode-electrolyte interactions in sensors. The specific surface area and pore size distribution of the CuO NF and NR were measured by performing BET surface area analysis. Fig. 3f shows the N_2 adsorption and desorption curves of CuO NF and NR for analysing the specific surface area of the samples. The curves indicate the type III isotherm behaviour with H3 type hysteresis at high relative pressures due to the multilayer adsorption with specific surface area of 29 m^2/cc for CuO NR and 28 m^2/g for CuO NF. Further, the pore size distribution was estimated using the adsorption and desorption isotherms using BJH and de Boer's method. As shown in Fig. 3f and 3g, the samples exhibited pore size distribution between 2 to 25 nm and this reveals the mesoporous (> 2 nm) nature of the samples. The average pore diameter of 8 nm and 9 nm were noted for

NR and NF respectively. The influence of pore size on sensing was studied with electrochemical impedance spectroscopic analysis and is discussed in the following section. The surface roughness of the printed film is very important in an electrochemical application for adsorption and desorption of ions. Fig. 3h and 3i show the 3D AFM images of the CuO NR and CuO NF. The root mean square surface roughness of the films was found to be 130 nm for CuO NR and 192 nm for CuO NF.

3.2.Electrochemical analysis of CuO NF and NR films

Most of the electrochemical studies of CuO so far have used either conventional two electrodes (sensitive and reference electrode) or three electrodes configuration (working electrode, Ag/AgCl reference electrode, and counter electrode) systems for measurements [8, 9, 23]. Here we have used a simple two-electrode configuration with IDE structure. As the CuO nanostructures with different morphologies have been used, the electrochemical performance is expected to vary because of changes in specific surface areas and porous nature. The EIS analysis was conducted for CuO NR and CuO NF electrodes in solutions with different pH values to investigate the sensing mechanism. When 10 mV voltage is applied across IDE, the local electrical field generated on each digit induces the changes in the electrical properties of the sensitive layer on the top [24, 25]. While varying the pH value of the solution, the positive (H^+ ion) or negative (OH^- ion) charged surface groups of the Electrical Double Layer (EDL) formed at the interface of CuO-electrolyte gets disturbed and this leads to change in the electrical properties of the sensitive layer [24], as shown in Fig. 4a. The higher concentration of H^+ or OH^- ions in the solution attenuates the external local electric field of the material. Due to the applied potential (10 mV) across ions in the solution are diffused/adsorbed into the electrodes and causes changes in the electrical properties such as complex impedance or capacitance [4, 18, 25].

The comparison of changes in capacitance with frequency in CuO NR and NF at pH 7 solution is shown in Fig. 4b. The capacitance decreases with increase in frequency. In addition, we observed that CuO NR based sensor have high capacitance than sensors based on CuO NF. This is also reflected in Fig. 4c, which shows the decrease in capacitance with increase in the pH value of the solution at selected frequencies (20, 50 and 100 Hz). The CuO NR based sensors show high sensitivity than CuO NF film-based sensor especially in the range of pH 5-8.5. Moreover, the high active surface area of CuO NR leads to better sensitivity, a slope of

0.64µF/pH at 50 Hz, as shown in Fig. 4d. However, for CuO NF, a large shift in capacitance with pH value of solution is observed

The diffusion/adsorption of ions in the sensitive material depends on the structure, nature of porosity, and the surface roughness of the materials [26, 27]. This can be determined from the EIS data presented as Nyquist plot in Fig. 5a for both electrodes. This shape of the Nyquist plot for the CuO NR and NF based pH sensor is different with respect to previous works such as those based on RuO_2 based pH sensor, where a bigger semi-circular arc in low frequency range is observed due to adsorption of ions on the surface of the electrode [24]. The semicircle which is observed in the higher frequency range of Nyquist plot, in Fig. 5a is assigned to the charge-transfer process of H^+/OH^-ions at the CuO/solution interface. This charge transfer resistance, (R_{ct}), is reflected by the diameter of the smaller semi-circle. The value of R_{ct} is related to the properties of the electrode material and is reversely proportional to the number of electrons participating in the electrode reaction [24]. Differently, from CuO NR, an incomplete semi-circle is observed in the case of CuO NF, as shown in Fig. 5a. It may be due to the surface roughness of nanomaterial. As observed in AFM images in Fig. 3h and 3i, the surface roughness of the CuO NF is greater than CuO NR. Moreover, it was observed that the NR CuO electrode exhibits smaller semicircles with an R_{ct} value of nearly 86 Ω in comparison with the CuO NF of 122 Ω, indicating a lower charge transfer resistance of the CuO NR electrode. This R_{ct} value was calculated by fitting with equivalent circuit (standard Randles circuit is shown in inset of Fig. 5a) analysis of the impedance data. This lower R_{ct} is possibly due to morphology of NRs, which are smaller in crystalline size have better contact with the solution than the NFs.

Furthermore, the nonzero intersection of the semi-circle with the real axis at the high frequency side is due to the solution resistance (R_s) and ohmic resistance of CuO film. The plots in Fig. 5a shows that this total resistance of CuO NR film is smaller (~119 Ω) than that of CuO NF film (~126 Ω) in the high frequency region. Even though the R_s is constant the variation in total resistance of CuO NR and NF electrode/solution interface is due to the ohmic resistance of the material. The smaller the ohmic resistance better the contact between the solution and the surface of CuO layer which will further improve the sensing performance of an electrochemical sensor. Further, the Nyquist plot for CuO NR was obtained with selected pH values of the solution. The variation of ionic concentration (such as H^+ or OH^- ions) on the value of R_{ct} is shown in Fig. 5b. It can be seen (from the inset of Fig. 5c) that the value of R_{ct} show the highest values for the solution with pH = 3 and decreases with increase in the basicity

of the solution. Compared to acidic and basic solution, at pH 7 the sensors have smaller semi-circle and hence the smallest value of R_{ct}.

The straight line in the lower frequency section could be attributed to the limited diffusion of H^+/OH^- into nanostructured CuO electrodes. It was found that the impedance related to the diffusion of ions in the solution through the pores of the NR and NF electrode depends on the morphology of material and pH value of the solution, as illustrated in Fig. 5a. The straight line is observed at 49º for CuO NR (shown in Fig. 5d) and 41º for CuO NF electrode. As compared to standard Warburg impedance (angle must be 45°) the observed angle for CuO varies with pH of solution. This variation in angle is due to the change in impedance value as a result of changes in the ionic concentration of the solution. In addition, the observed changes in the angles are due to variations in pore structure, shape and dimension of the nanomaterials [27], which are also observed in the BET analysis, shown in Fig. 3g. The angle of the straight line at low frequency varies with changes in pH value of the solution (inset of Fig. 5d). For example, in the case of CuO NR electrode the angle for the straight-line increases in acidic region (from pH 2 to pH 7) between 30 to 49°. However, for the basic region the angle is almost constant (about 47°). This distinct pH dependent changes characteristics at an acidic solution is related to the H^+ diffusion, as acidic solutions contain more H^+ ions. This clearly explains that the impedance variation of the nanomaterial not only depends on the pore dimension or structure, but it is also strongly influenced by the ionic concentration of the solution. As compared to acidic and basic solution, the concentration of active ions such as H^+ or OH^- is lower in neutral and slightly basic region. Fig. 4b confirms that the capacitance almost varies linearly with pH in neutral and basic regions. Moreover, due to high ohmic and charge transfer resistance the CuO NF morphology with respect to CuO NR, the sensor shows low sensitivity in the neutral and slightly basic region of solution.

The EIS results, presented as Bode impedance and phase angle plots (log|Z| - logF and Φ - logF) in Fig. 5e, show that at high frequencies the impedance decreases, and the phase angle tends to have lower magnitude. At lower frequencies, the increase of log|Z|, with decreasing logF and phase angle, is higher and this indicates the capacitive reactance behaviour of the sensor performance. The variations in impedance or capacitance of the CuO NR and NF in the low frequency range are suggested in Fig. 4c, arise mainly from diffusion of ions and depends on the shape of nanostructure, porosity, and ionic concentration, while in the higher frequency range it depends on the ionic concentration of the solution and surface nature of the material.

To evaluate the performance of sensors under stable conditions we also tested them in standard buffer solution with pH values in the range of 5-9 which is important for water, food quality, agricultural, etc. We found that the conductivity of solution varied with any change in the solution. Due to presence of salts in buffer solution, the conductivity is higher with respect to other solutions based on distilled water with HCl/KOH. We observed that the solution conductivity influences the sensor performance and can be studied by measuring the value of solution resistance. Fig. 5f shows the Nyquist plot at high frequency range and the solution resistance is lower in comparison with Fig. 5c. In both solutions, the sensor shows a stable performance, however, there is change in the electrical parameters.

The sensitivity from Fig. 4d indicates that NR based sensors are more effective than NF based sensors. Based on above EIS examination of CuO NF and CuO NR electrode results, we can conclude that in addition to nature and morphology of the material the mixed ionic and electronic conduction is responsible for the observed EIS variation of CuO NF and NR electrode. This aligns with results reported in the literature, where an identical electrochemical behaviour was observed for CuO NF morphology based glucose sensors[23] and electrochemical supercapacitors[7]. Comparison of CuO based pH sensors are presented in Table 1. From our studies, we also observed that the presented sensors may not be suitable for long-term use as the binder gets removed from the thick film paste during reaction with pH solution. This indicates that perhaps the most suitable immediate use of our sensors will be in disposable systems.

The major advantages of the presented CuO nanostructures based approach are that the sensor can be fabricated at low temperatures, which helps overcome the traditional issue related to thermal budget in the case of flexible electronics. To demonstrate the efficacy of presented approach for flexible electronic systems, we have tested the flexible sensor by fitting them inside a small cylinder and conforming to the curved surface as shown in Fig. 6a. By keeping a constant pH solution (buffer solution of pH 7) the diameter of the cylinder was varied. Fig. 6b represents the variation of capacitance with frequency for different bending conditions. The change in electrochemical parameters with different bending conditions is presented in Table 2. It was found that the capacitance value decreases with increase in radius of curvature of bending. This variation of capacitance was clearly observed from the EIS analysis also. The total resistance (i.e. due to the solution resistance and ohmic resistance of CuO film) at the nonzero intersection of the semi-circle with the real axis at the high frequency side was measured as 201 Ω, 198 Ω and 187 Ω respectively for F0, F1 and F2. The solution is same

during the measurement, so the influence of the solution resistance is constant. Hence, the observed variation in resistance before and after bending is due to the variation of electrical properties of the nanostructured film. It is clearly observed from the Nyquist plot of Fig. 5c the diameter of the semicircle arc is varying during bending. The surface area of the film is changing while bending and it influences the charge transfer resistance of the film. With increased bending the sensor R_{ct} value increases as shown in Figure 6c. Furthermore, in the low frequency range it was observed that the angle at the straight line is 23° without bending, 30° for 5 mm bending, and 33° when the electrode is bend at 10 mm radius of curvature. The change in slope of the lines at a low frequency while bending is related to the change in diffusion resistance of the ions in the pores which is present in the electrode.

For all these application, the solution will contain different analytes and reagents. To test the performance for different type of solution the presented the CuO NR based flexible sensor was also tested in DMEM solution in addition to buffer solution and distilled water, and varying pH value between 5.5 and 8.5. The sensor performance for pH 5.5, 6.8 and 8.5 are sown in Fig. 6d. A large shift in capacitance is observed at basic pH value of the solution. As compared to the measurement in HCl and KOH solution it was observed that the solution medium has an influence on the sensing performance. In low frequency range (below 100 Hz, shown in the inset of the Fig. 6d) a disturbance in capacitance is observed. It may be due to the presence of interference of other components in the DMEM solution including bicarbonate. Furthermore, reduction in the capacitance is observed with DMEM solution as compared to pH test solution. This may be due to the influence of amino acids and vitamins in DMEM that adjust their charge upon pH variations and thus alter the resistivity of the medium. To overcome the issues in influence of proteins or other reagents in biological application a further modification on the sensitive electrode is necessary.

The performance of sensor under test solution (pH 7) was evaluated by varying the potential of sinusoidal signal (5, 10, 50 and 100 mV) and the resulting variation of total impedance is presented in Fig. 6e. It was observed that this sinusoidal signal influences the EIS analysis. In majority of biomedical applications, the applied sinusoidal potential is in the range of 5 to 10 mV. Here, we have tested the sensor in 5 to 100 mV and the sensor showed stable performance. However, we also observed a slight variation in the capacitance due to interference of other ions and redox analytes from solution to the SE. The performance interference of ions such as Na^+, K^+ and analytes such as urea on the capacitance of sensors were measured and compared with selected frequencies, as shown in Fig. 6f. From this

analysis, we observed an average of ±1.5nF variation in capacitance due to the interference from other ions and analytes. However, solution resistance shows significant interference with other ions than the analytes. The sensor shows solution resistance in the range of 2.8 kΩ with or without glucose and urea. However, when salts of Na^+ and K^+ ions are added to the solution, the solution resistance drastically reduced in the range of 500 Ω. This can be attributed to change in the conductivity of solution when salt is added. Nanostructured CuO was also evaluated for non-enzymatic glucose sensors [14]. Here we tested the influence of ions and analytes with 0.01M concentration, however for real sample analysis the concentration is in the range of mM and in such conditions the influence on sensor performance will be insignificant. From our studies, we also observed that the reactions with pH solution also removed some of binder from the thick film and this means the most suitable use of proposed sensors will be in disposable systems. As a future work, we plan to study the performance of presented sensors in different cell culture medium and fabricate flexible/ stretchable pH sensors [28, 29] that also have longer life time. For this purpose, we will also investigate more morphologies for CuO nanostructures and composites.

Conclusion

In conclusion, the CuO nanorods based electrochemical pH sensors have been presented here and their performance has been evaluated with respect to previously reported nanoflower based sensors. The low temperature synthesis using a hydrothermal method and screen printing technology has been explored as they are suitable for flexible electronics technology. The crystalline porous CuO NR and NF sensors were found to exhibit excellent sensor performance in terms of capacitance and impedance. The NR based sensors show higher capacitance and better stability than NF based sensor. The evaluation of CuO nanorods based sensors for various bending conditions (radius of curvature of 10 mm and 5 mm) indicates that capacitance decrease almost linearly with increase in bending. The impedance spectroscopic analysis of sensitive layer shows that in the low frequency region ions are diffused in the surface material and causes Warburg impedance. In high frequency range charge transfer resistance plays an important role in pH sensing and in low frequency range ionic diffusion plays an important role in pH sensing. The presented sensors with further modification on the surface of the sensitive electrode could be used in biological applications. As a future work,

we plan to study the performance of our sensors in different cell culture medium and fabricate sensors for longer operations.

Acknowledgements

This work was partially supported by EPSRC Engineering Fellowship for Growth under Grant (EP/M002527/1). Authors are grateful to Prof. Dorota Szwagierczak Institute of Electron Technology, Krakow Division, 30-701 Krakow, Zablocie 39, Poland for supporting the fabrication of sensors.

References

[1] S. Zhuiykov, Solid-state sensors monitoring parameters of water quality for the next generation of wireless sensor networks, Sensor. Actuat. B: Chem., 161 (2012) 1-20.
[2] T. Guinovart, G. Valdés-Ramírez, J. R. Windmiller, F. J. Andrade, J. Wang, Bandage-Based Wearable Potentiometric Sensor for Monitoring Wound pH, Electroanal., 26 (2014) 1345-1353.
[3] C. Nie, A. Frijns, M. Zevenbergen, J. d. Toonder, An integrated flex-microfluidic-Si chip device towards sweat sensing applications, Sensor. Actuat. B: Chem., 227 (2016) 427-437.
[4] K. Arshak, E. Gill, A. Arshak, O. Korostynska, Investigation of tin oxides as sensing layers in conductimetric interdigitated pH sensors, Sensor. Actuat. B: Chem., 127 (2007) 42-53.
[5] P. Kurzweil, Metal oxides and ion-exchanging surfaces as pH sensors in liquids: State-of-the-art and outlook, Sensors., 9(2009) 4955-4985.
[6] Y. Qin, H.-J. Kwon, M. M. Howlader, M. J. Deen, Microfabricated electrochemical pH and free chlorine sensors for water quality monitoring: recent advances and research challenges, RSC Adv., 5 (2015) 69086- 69109.
[7] B. Heng, C. Qing, D. Sun, B. Wang, H. Wang, Y. Tang, Rapid synthesis of CuO nanoribbons and nanoflowers from the same reaction system, and a comparison of their supercapacitor performance, RSC Adv., 3 (2013) 15719-15726.
[8] S.-P. Chang, T.-H. Yang, Sensing performance of EGFET pH sensors with CuO nanowires fabricated on glass substrate, Int. J. Electrochem. Sci., 7 (2012) 5020 - 5027.
[9] S. Zaman, M. H. Asif, A. Zainelabdin, G. Amin, O. Nur, M. Willander, CuO nanoflowers as an electrochemical pH sensor and the effect of pH on the growth, J. Electroanal. Chem., 662 (2011) 421-425.
[10] Q. Zhang, K. Zhang, D. Xu, G. Yang, H. Huang, F. Nie, et al., CuO nanostructures: Synthesis, characterization, growth mechanisms, fundamental properties, and applications, Prog. Mater. Sci., 60(2014) 208-337.
[11] M. L. Zhong, D. C. Zeng, Z. W. Liu, H. Y. Yu, X. C. Zhong, W.Q. Qiu, Synthesis, growth mechanism and gas-sensing properties of large-scale CuO nanowires, Acta Mater., 58 (2010) 5926-5932.
[12] C.-L. Hsu, J.-Y. Tsai, T.-J. Hsueh, Ethanol gas and humidity sensors of CuO/Cu_2O composite nanowires based on a Cu through-silicon via approach, Sensor.Actuat. B: Chem. 224, (2016) 95-102..
[13] K. Mageshwari, R. Sathyamoorthy, Flower-shaped CuO nanostructures: synthesis, characterization and antimicrobial activity, J. Mater. Sci. Technol., 29 (2013) 909-914.
[14] L.-C. Jiang, W.-D. Zhang, A highly sensitive nonenzymatic glucose sensor based on CuO nanoparticles-modified carbon nanotube electrode, Biosensor. Bioelectron., 25 (2010) 1402-1407.
[15] E. Comini, Metal oxide nanowire chemical sensors: innovation and quality of life, Mater. Today, 19 (2016) 559-567.
[16] A. Liu, Towards development of chemosensors and biosensors with metal-oxide-based nanowires or nanotubes, Biosensor. Bioelectron., 24 (2008) 167-177.
[17] S. Khan, L. Lorenzelli, R. S. Dahiya, Technologies for printing sensors and electronics over large flexible substrates: A Review, IEEE Sensor. J., 15 (2015) 3164-3185.
[18] M. Simić, L. Manjakkal, K. Zaraska, G. M. Stojanović, R. Dahiya, TiO_2-based thick film pH sensor, IEEE Sensor. J., 17 (2016) 248-255.
[19] L. Debbichi, M. C. Marco de Lucas, J. F. Pierson, P. Krüger, Vibrational properties of CuO and Cu_4O_3 from first-principles calculations, and raman and infrared spectroscopy, J. Phys. Chem. C, 116 (2012) 10232-10237.

[20] Y. Cudennec, A. Lecerf, The transformation of $Cu(OH)_2$ into CuO, revisited, Solid State Sci., 5(2003) 1471-1474.
[21] D. P. Volanti, M. O. Orlandi, J. Andres, E. Longo, Efficient microwave-assisted hydrothermal synthesis of CuO sea urchin-like architectures via a mesoscale self-assembly, CrystEngComm, 12 (2010) 1696-1699.
[22] F. Haiming, Z. Bingsuo, L. Yulong, X. Sishen, Size effect on the electron–phonon coupling in CuO nanocrystals, Nanotechnol., 17(2006) 1099.
[23] L.-C. Jiang, W.-D. Zhang, A highly sensitive nonenzymatic glucose sensor based on CuO nanoparticles-modified carbon nanotube electrode, Biosensor. Bioelectron. 25 (2010) 1402-1407.
[24] L. Manjakkal, E. Djurdjic, K. Cvejin, J. Kulawik, K. Zaraska, D. Szwagierczak, Electrochemical impedance spectroscopic analysis of RuO_2 based thick film pH sensors, Electrochim. Acta, 168 (2015) 246-255.
[25] L. Manjakkal, K. Cvejin, J. Kulawik, K. Zaraska, R. P. Socha, D. Szwagierczak, X-ray photoelectron spectroscopic and electrochemical impedance spectroscopic analysis of RuO_2-Ta_2O_5 thick film pH sensors, Anal. Chim. Acta, 931(2016) 47-56.
[26] V. F. Lvovich, Impedance spectroscopy: applications to electrochemical and dielectric phenomena: John Wiley & Sons; 2012.
[27] D. D. Macdonald, Reflections on the history of electrochemical impedance spectroscopy, Electrochim. Acta, 51 (2006) 1376-1388.
[28] W. Dang, V. Vinciguerra, L. Lorenzelli, R. Dahiya, Printable stretchable interconnects. Flex. Print. Electron., 2, 013003, 2017.
[29] W. Dang, L. Manjakkal, L. Lorenzelli, V. Vinciguerra, R. Dahiya, Stretchable pH sensing patch in a hybrid package. In: IEEE Sensors 2017, Glasgow, UK, 30 Oct - 01 Nov 2017.

Author biography

Libu Manjakkal: Received B.Sc. degree in physics from Calicut University, India, in 2006, the M.Sc. degree in physics from Mahatma Gandhi University, India, in 2008, and the Ph.D. (Hons.) degree in Electronic Engineering from the Institute of Electron Technology, Warsaw, Poland, in 2015. His Ph.D. thesis was related to metal oxide based thick film pH sensors. From 2009 to 2012, he was involved in two research and development projects with the Center for Materials for Electronics Technology, Thrissur, India. In 2012, he was with CEMOP/UNINOVA, New University of Lisbon, Portugal. From 2012 to 2015, he was an Early Stage Research Fellow in the framework of Marie Curie ITN Program within the SENSEIVER Project, ITE. From 2015 to 2016, he was a Post-Doctoral Researcher with ITE. In 2016, he was a Marie Curie Experienced Researcher with Electronics and Nanoscale Engineering Research Division, BEST Group, University of Glasgow, U.K., where he is currently a Post-Doctoral Fellow with the EPSRC Project PRINTSKIN. He has authored or co-authored 28 scientific papers. His current research interests comprise flexible and printable electronics, supercapacitors, electrochemical sensors, LTCC technology, multilayer actuators, TCO films, pH sensors, and gas sensors.

Bhuvaneshwari Sakthivel: Received the bachelor's degree in physics from the PSG College of Arts and Science, Bharathiyar University, in 2010, the master's degree in physics from the National Institute of Technology, Tiruchirappalli, India, in 2012, and the Ph.D. degree in the field of metal oxide semiconductors for gas sensing applications from the National Institute of Technology, Tiruchirappalli, where she is currently pursuing the Ph.D. degree with the Department of Physics

Gopalakrishnan Nammalvar: Received the B.Sc. and M.Sc. degrees in physics from Madhurai Kamarajar University, in 1988 and 1990, respectively, the M.Phil. and Ph.D. degrees from Anna University, Chennai, India, in 1991 and 1997, respectively. He is currently an Associate Professor with the Department of Physics, National Institute of Technology, Tiruchirappalli, India. He was a Post-Doctoral Researcher with universities in Sweden (KTH), Japan (AIST), and South Korea (DEU). His current research interests include the growth of III–V and II–VI semiconductor thin films and nanostructures for optoelectronics, spintronics, and gas sensing applications. He was a recipient of the prestigious STA Fellowship offered by the Japan Science and Technology Association for Crystal Growth. He is a Life Member of the Indian Association for Crystal Growth, the Magnetic Society of India, and the Indian Society for Non-Descriptive Technique.

Ravinder Dahiya is Professor of Electronics and Nanoengineering in the University of Glasgow, U.K. He is the leader of Bendable Electronics and Sensing Technologies (BEST) research group, which conducts fundamental and applied research in the multidisciplinary fields of flexible and printable electronics, tactile sensing, electronic skin, robotics and wearable systems. He has authored over 170 research articles, 4 books (including 3 in various stages of publication), and 9 patents (including 7 submitted). He has worked has led several international projects. He is a Distinguished Lecturer of the IEEE Sensors Council. He is serving on the editorial boards of the Scientific Report, IEEE TRANSACTIONS ON ROBOTICS and the IEEE SENSORS JOURNAL. He is the Founding Chair of the IEEE UKRI Sensors Council Chapter and the Technical Program Chair of the IEEE Sensors 2017 and IEEE Sensors 2018. He holds the prestigious EPSRC Fellowship and received in past the Marie Curie

Fellowship and Japanese Monbusho Fellowship. He received the 2016 Technical Achievement Award from the IEEE Sensors Council, the International Association of Advanced Materials Medal for 2016, and the 2016 Microelectronic Engineering Young Investigator Award. He received best paper awards two times and another two second best paper awards as a co-author in international conferences.

Figure Caption

Fig. 1: (a) Flow chart for synthesis of CuO NR and CuO NF (b) schematic representation of CuO based IDE pH sensor and (c) image of the flexible CuO based pH sensor.

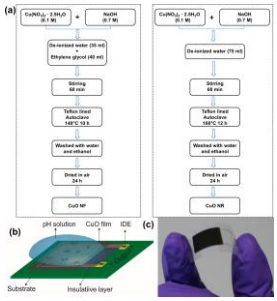

Fig. 2: Surface and structural morphologies of CuO nanostructures (a) - (c) FESEM, TEM images and SAED pattern of CuO NF, (d) –(f) FESEM, TEM image SAED pattern of CuO NR.

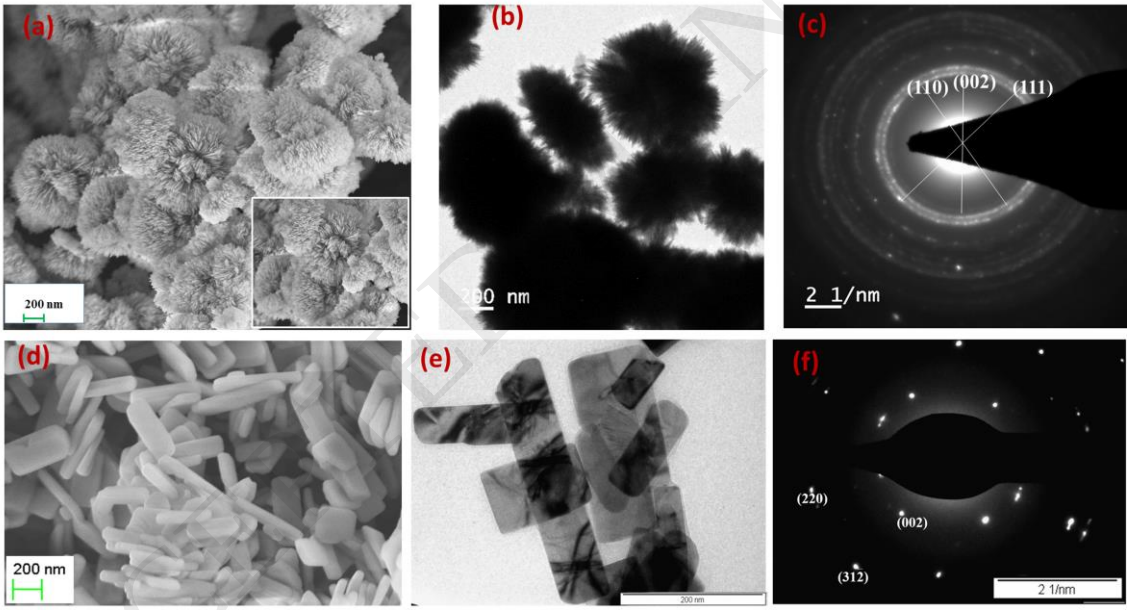

Fig. 3: Crystal structure, phase group and functional group analysis of CuO nanostructures; (a) and (b) X-ray diffraction pattern of CuO NF and NR powder, (c) and (d) Raman spectra of CuO NF and NR film (e) FTIR spectra of CuO NF and NR powder, (f) N_2 adsorption - desorption curves of CuO NR and NF (g) pore size distribution calculated from de-Boer's method for CuO NF and NR with inset for CuO NR, and AFM images of (h) CuO NF and (i) CuO NR films.

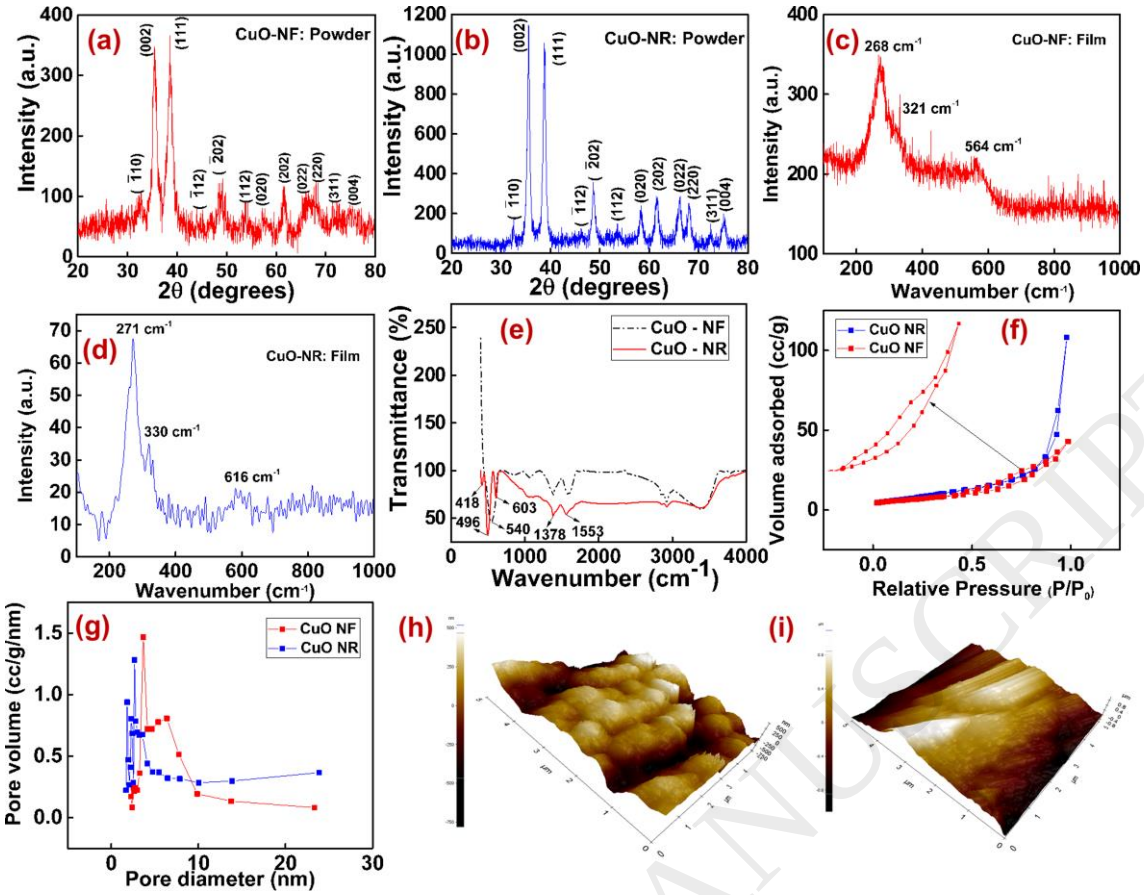

Fig. 4: (a) Electrochemical double layer formation of CuO nanomaterial/solution interface, (b) comparison of variation of capacitance with frequency at pH 7 for CuO NF and NR (c) the change in capacitance with pH of solution for CuO NR and NF at 50 and 100 Hz and (d) the change in capacitance in the region of pH 5 to 8.5 for CuO NR and NF at 50 Hz.

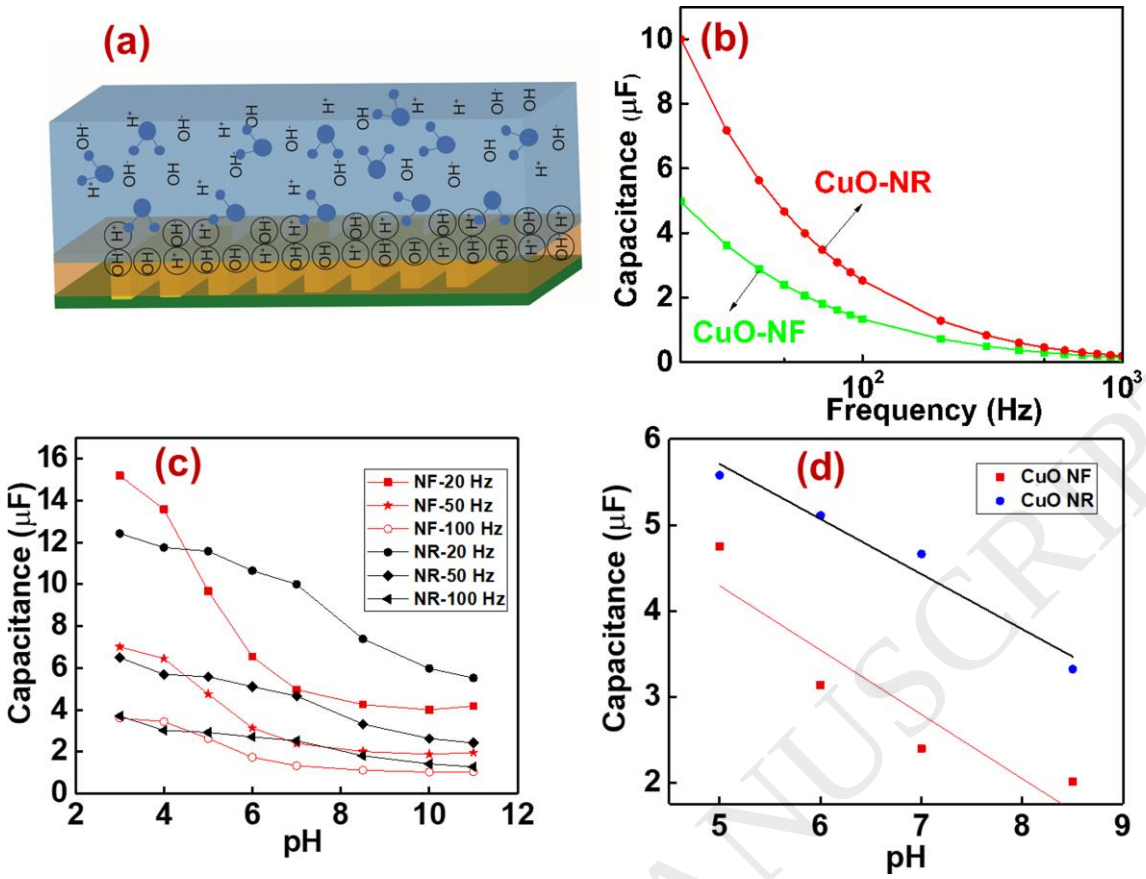

Fig. 5: Electrochemical reaction at the interface of electrode-electrolyte (a) Nyquist plot for CuO NR and CuO NF at pH 7 (inset shows the equivalent circuit; R_{ct}- charge transfer resistance, R_s-solution resistance and ohmic resistance; C_{dl}- double layer capacitance and W-Warburg impedance), (b) Nyquist plot for selected pH value of CuO NR, (c) the Nyquist plot for high frequency (d) the angle for the straight line at low frequency section of Nyquist plot (the inset shows the variation of this angle with pH of solution), (e) comparison of the Bode impedance and phase angle for CuO nanomaterial and (f) Nyquist plot for buffer solution with selected pH value of CuO NR

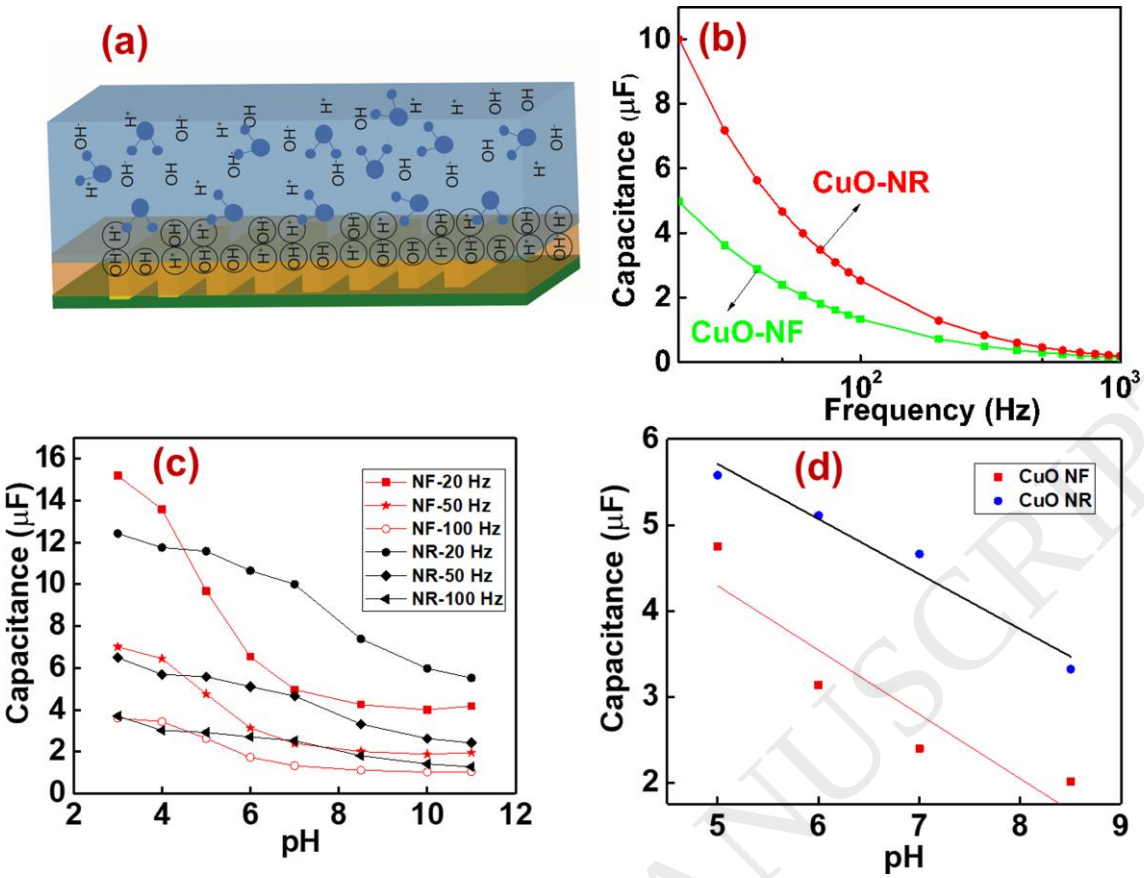

Fig. 6: (a) Image of flexible sensor in a tube with a radius of curvature 5mm for testing the EIS performance, inset represent the schematic representation, (b) capacitance variation with frequency for different bending of the sensor (F-0: without bending, F-1, and F-2, with bending at a radius of curvature 5 mm, and 10 respectively), (c) Nyquist plot of senor during different bending condition, (d) the variation of capacitance CuO NR based sensor in DMEM (e) influence of interference of ions and analytes for selected frequencies and (f) influence of applied sinusoidal signal potential on the flexible pH sensor.

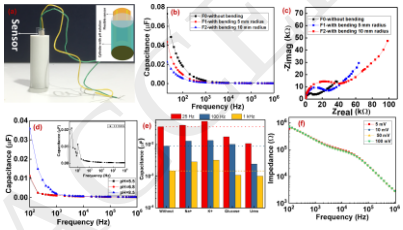

Table 1: Comparison of CuO based pH sensors

Morphology	Method of fabrication of material	Type of sensor	Performance	Ref
CuO NF	Low-temperature chemical bath method	Potentiometric	28 mV/pH in the range of pH 2-11	[9]
CuO nanowire (CuO NW)	Thermally annealing of Cu film at 450 °C for 5 h in air	Extended-gate field-effect-transistor (EGFET)	23.5 μA/pH and 18.4 mV/pH in the range of pH 4-10	[8]
CuO NF	Hydrothermal synthesis	Interdigitated impedancemetric	Capacitance decrease with increasing pH for low frequency (at pH 7 2.34μF for 50Hz)	This work
CuO NR	Hydrothermal synthesis	Interdigitated impedancemetric	Capacitance decrease with increasing pH for low frequency (at pH 7, 4.64μF for 50Hz)	This work

Table 2: Comparison of performance of flexible pH sensors in different bending conditions

Flexibility	Radius of curvature (RC)	Capacitance (at 20Hz) (nF)	Solution resistance (Rs) (Ω)	Phase angle (°)
F0	Without bending	70	201	23
F1	With 5 mm RC of bending	40	198	30
F2	With 10mm RC of bending	20	187	33